Journal of Solid State Chemistry 183 (2010) 2855–2861

Contents lists available at ScienceDirect

Journal of Solid State Chemistry

journal homepage: www.elsevier.com/locate/jssc

Phase equilibria of the Ba–Sm–Y–Cu–O system for coated conductor applications

G. Liu [a], W. Wong-Ng [a,*], Z. Yang [a], J.A. Kaduk [b], L.P. Cook [a,c]

[a] Ceramics Division, Materials Science and Engineering Laboratory, National Institute of Standards and Technology, Gaithersburg, MD 20899, USA
[b] Poly Crystallography Inc., Naperville, IL 60540, USA
[c] PhazePro Technologies LLC, Hustontown, PA 17229, USA

ARTICLE INFO

Article history:
Received 1 February 2010
Received in revised form
20 July 2010
Accepted 1 September 2010
Available online 8 September 2010

Keywords:
Ba–Sm–Y–Cu–O phase diagrams
$(Ba_{2-x}Sm_x)(Sm_{1-y}Y_y)Cu_3O_{6+z}$ solid solution
Coated conductors

ABSTRACT

The complex phase relationships near the BaO-poor region of the quaternary Ba–Sm–Y–Cu–O oxide system prepared in pure air ($p_{O_2}=22$ kPa, 950 °C) and in 0.1% O_2 ($p_{O_2}=100$ Pa, 810 °C) have been determined. This investigation also included the subsolidus compatibilities in ten subsystems (Ba–Sm–Y–O, Ba–Sm–Cu–O, Ba–Y–Cu–O, Sm–Y–Cu–O, Ba–Sm–O, Ba–Y–O, Ba–Cu–O, Sm–Y–O, Sm–Cu–O, and Y–Cu–O), and the homogeneity range of five solid solutions ($Ba(Sm_xY_{2-x})CuO_5$, $(Sm,Y)_2O_3$, $(Sm,Y)_2CuO_4$, $(Y,Sm)_2Cu_2O_5$, and $Ba(Sm,Y)_2O_4$). The single phase range of the superconductor solid solution, $(Ba_{2-x}Sm_x)(Sm_{1-y}Y_y)Cu_3O_{6+z}$, and the phase compatibilities in its vicinity, which are particularly important for processing, are described in detail. The phase equilibrium data of the Ba–Sm–Y–Cu–O system will enable the improvement of the intrinsic superconducting properties of second-generation wires, and facilitate the flux-pinning process.

Published by Elsevier Inc.

1. Introduction

Current economic and environmental issues demand improvements in electrical distribution grids for more efficient utilization of energy resources. High-temperature superconductors have demonstrated potential for meeting these needs [1]. There is continued effort within the high T_c community on research and development of coated conductors for wire and tape applications [2–7]. These coated conductors are based on $Ba_2YCu_3O_{6+z}$ (Y-213) and $Ba_2RCu_3O_{6+z}$ (R-213, R=lanthanides) as the principal superconductors. Y-213 and R-213 can be deposited on flexible substrates using various approaches, including the BaF_2 technique [8–14]. The resulting tapes show excellent current-carrying capability. Phase equilibrium data on the multi-component phase relationships of mixed lanthanide high temperature superconductor phases are important for coated conductor wire/tape processing.

Since an understanding of the detailed multi-component phase equilibrium relationships in the vicinity of the superconductor solid solutions will facilitate optimization of coated conductor processing, our goal is to provide critical data for these single phase solid solutions. Such data will enable improvement of the intrinsic superconducting properties of second-generation wires and the associated flux-pinning processes. For example, one can tailor superconducting and melting properties of the mixed lanthanide 213 solid solutions by substitution of larger lanthanides on the Ba site, and also by mixing larger lanthanide ions (R) with smaller ones (R'). MacManus-Driscoll et al. reported that compositions in the $(Ba_{2-x}Sm_x)(Sm_{1-y}Y_y)Cu_3O_{6+z}$ system give rise to enhanced J_c properties [15]. The compatibilities of this solid solution with its neighboring phases are crucial as a reference for coated conductor processing as well as for property investigations.

This paper reports the complex phase equilibria of the Ba–Sm–Y–Cu–O system as well as the single phase solid solution region of $(Ba_{2-x}Sm_x)(Sm_{1-y}Y_y)Cu_3O_{6+z}$. Since X-ray patterns are important to serve as standards for phase analysis, we have also prepared reference X-ray powder diffraction patterns of selected solid solutions in the $(Ba_{2-x}Sm_x)(Sm_{1-y}Y_y)Cu_3O_{6+z}$ and $Ba(Sm_xY_{2-x})CuO_5$ systems to be included in the Powder Diffraction File (PDF, produced by the International Centre for Powder Diffraction (ICDD) [16]).

2. Experimental[1]

2.1. Sample synthesis

Ten end members that constitute various multi-component regions in the Ba–Sm–Y–Cu–O system were synthesized and used as master batches for preparing nine individual batches of $Ba_2SmCu_3O_{6+z}$, $Ba_2YCu_3O_{6+z}$, $BaSm_2CuO_5$ (Sm-121), BaY_2CuO_5 (Y-121), $BaSm_2O_4$, BaY_2O_4, Sm_2CuO_4, $Y_2Cu_2O_5$, and $BaCuO_2$. These

* Corresponding author.
E-mail address: Winnie.wong-ng@nist.gov (W. Wong-Ng).

0022-4596/$ - see front matter Published by Elsevier Inc.
doi:10.1016/j.jssc.2010.09.001

master batches were prepared by heat-treating a stoichiometric mixture of $BaCO_3$, Sm_2O_3, Y_2O_3, and CuO. Samples were weighed out with < 1.0% (relative) estimated uncertainty for component compositions of 10–100 mol%, and < 5% (relative) estimated uncertainty for component compositions with less than 10 mol%. Following this, samples were well-mixed and calcined first at 850 °C, followed by final annealing at 900–1000 °C for about 15 days with intermediate grindings to ensure single phase properties. Samples were prepared using different combinations of these nine master batches as well as using Y_2O_3, Sm_2O_3, and CuO, depending on the equilibrium regions of the Ba–Sm–Y–Cu–O system under investigation (tables listing the 274 compositions investigated in this study have been deposited as Supplementary Tables (Tables S1–S3)). For samples prepared in air, the heat-treatment procedure was: 850 °C for 20 h, 900 °C for 20 h, 930 °C for 20 h, and 950 °C for 100–400 h with intermediate grindings. For samples prepared in $p_{O_2} = 100$ Pa, samples were heat-treated at 810 °C for 40–200 h with intermediate grindings.

To study the range of the solid solution $(Ba_{2-x}Sm_x)(Sm_{1-y}Y_y)Cu_3O_{6+z}$, two sets of 75 samples were prepared using high temperature solid state methods in $p_{O_2} = 100$ Pa (810 °C for 40–200 h) and in pure air (950 °C for 100–400 h) with intermediate grindings.

The experimental conditions used in this study were selected in consultation with an industry/university/government advisory group to correspond to processing parameters employed by those most active in developing high T_c products for wire and cable applications.

2.2. Phase identification using X-ray diffraction

X-ray powder diffraction was used to identify the phases synthesized, to confirm phase purity, and to determine phase relationships. A computer-controlled automated Philips diffractometer equipped with a θ-compensation slit and Cu$K\alpha$ radiation was operated at 45 kV and 40 mA. The radiation was detected by a scintillation counter and a solid-state amplifier. All X-ray patterns were measured using a hermetic cell designed for air-sensitive materials [17]. The Siemens software package and the reference X-ray diffraction patterns of the Powder Diffraction File (PDF) [16] were used for performing phase identification.

2.3. Structural studies and reference patterns

To study the structure and prepare X-ray reference patterns, the X-ray Rietveld refinement technique (GSAS Suite) [18,19] was applied (neutron diffraction was not used because of neutron absorption by Sm). The structures of selected $(Ba_{2-x}Sm_x)(Sm_{1-y}Y_y)Cu_3O_{6+z}$ and $Ba(Sm_xY_{2-x})CuO_5$ phases were determined using a Bruker XRD D8 Diffractometer equipped with a VANTEC-1 position-sensitive detector. Diffraction patterns were collected (Cu$K\alpha$ radiation, 40 kV, 40 mA, 0.3° divergence slit) from 8° to 140° 2θ using Ni-filtered Cu$K\alpha$ radiation, and counting for 0.3 s/step. The specimens were mounted as acetone slurries on zero-background cells, and were rotated rapidly during data collection. The background was described by a 6-term shifted Chebyshev function of the first kind.

Reference X-ray patterns of selected members of the $(Ba_{2-x}Sm_x)(Sm_{1-y}Y_y)Cu_3O_{6+z}$ and $Ba(Sm_xY_{2-x})CuO_5$ systems were prepared using a Rietveld pattern decomposition technique. These patterns represent ideal specimen patterns. They are corrected for systematic errors in both *d* and *I*. The reported peak positions are calculated from the refined lattice parameters, as these positions represent the best measure of the true positions. For peaks resolved at the instrument resolution function, the individual peak positions are reported. For overlapping peaks, the intensity-weighted average peak position is reported with multiple indices. For marginally resolved peaks, individual peaks are reported to more accurately simulate the visual appearance of the pattern.

[1] The purpose of identifying the equipment in this article is to specify the experimental procedure. Such identification does not imply recommendation or endorsement by the National Institute of Standards and Technology.

3. Results and discussion

The phase relations in the vicinity of BaO poor region of the Ba–Sm–Y–Cu–O system under both pure air ($p_{O_2} = 22$ kPa)

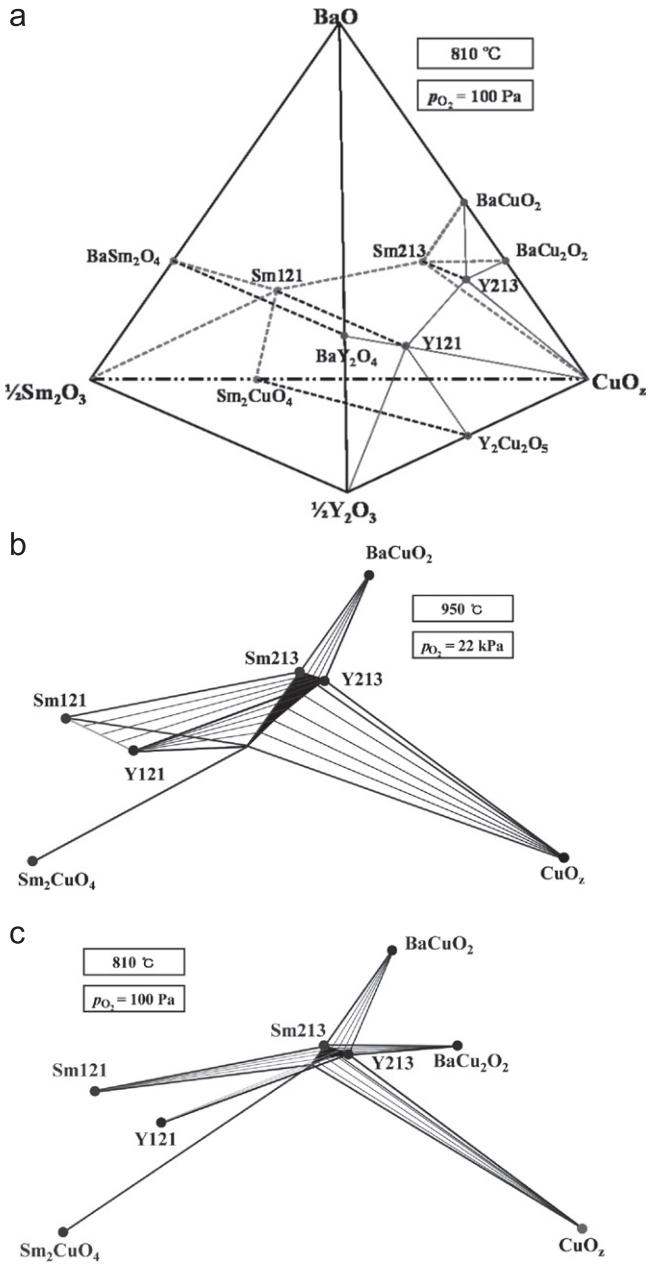

Fig. 1. (a) Phase diagram overview of the Ba–Sm–Y–Cu–O system in the BaO-poor region prepared in $p_{O_2} = 100$ Pa, 810 °C (overview prepared at $p_{O_2} = 22$ kPa, 950 °C is similar, without the presence of $BaCu_2O_2$), (b) schematic illustrating the tie line relationships in the vicinity of the $(Ba_{2-x}Sm_x)(Sm_{1-y}Y_y)Cu_3O_{6+z}$ solid solution at $p_{O_2} = 22$ kPa, 950 °C, and (c) schematic at $p_{O_2} = 100$ Pa, 810 °C.

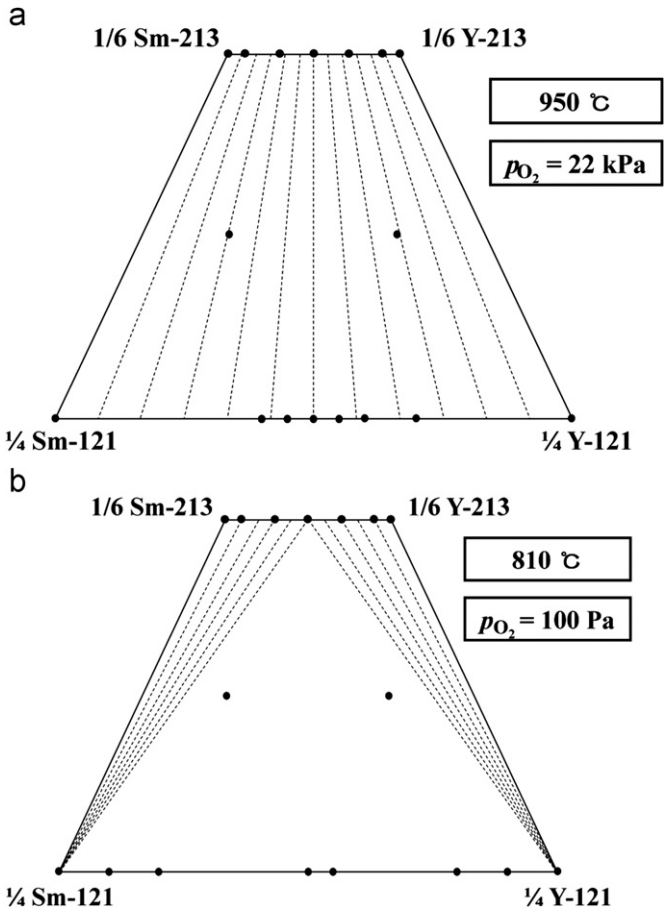

Fig. 2. Phase diagram of the $Ba_2SmCu_3O_{6+z}$–$Ba_2YCu_3O_{6+z}$–$BaSm_2CuO_5$–BaY_2CuO_5 system prepared in (a) pure air (p_{O_2} = 22 kPa, 950 °C) and (b) p_{O_2} = 100 Pa, 810 °C.

and p_{O_2} = 100 Pa are presented in Figs. 1–8. Because the $(Ba_{2-x}Sm_x)(Sm_{1-y}Y_y)Cu_3O_{6+z}$ phase is a solid solution, some of the tie-lines to the neighboring phases are in the form of tie-line bundles. The tie-line connections and tie-line bundles between these solid solutions were estimated using X-ray data for the experimental compositions plotted in the figures. The equilibria of the Ba–Sm–Y–Cu–O system under pure air and under p_{O_2} = 100 Pa are in general very similar except for the ranges of the solid solutions. Also, under p_{O_2} = 100 Pa, there is an additional reduced phase, $BaCu_2O_2$.

3.1. Ba–Sm–Y–Cu–O system

Before we describe the phase equilibria of the mixed lanthanide Ba–Sm–Y–Cu–O system, a brief review of the phase diagrams of the Ba–Sm–Cu–O [20] and Ba–Y–Cu–O systems [21] is useful, particularly the solid solution extent of the $(Ba_{2-x}Sm_x)(Sm_{1-y}Y_y)Cu_3O_{6+z}$ phase. It has been observed that under p_{O_2} = 100 Pa, because of the close match of ionic radius between Sm^{3+} and Ba^{2+} [22], there are several solid solution series in the diagram. Also, the solid solution range in $Ba_{2-x}Sm_{1+x}Cu_3O_{6+z}$ is much larger when the samples are prepared in pure air than in p_{O_2} = 100 Pa. In the case of Y-containing systems, since there is a substantial difference of ionic radius between Y^{3+} and Ba^{2+}, and Ba occupies a large cage in this structure, there is no detectable substitution of Y in the Ba site. A comparison of the Ba–Sm–Cu–O and the Ba–Y–Cu–O diagrams also reveals a difference in phase formation in the R–Cu–O systems. For example, the $Y_2Cu_2O_5$ phase was found in

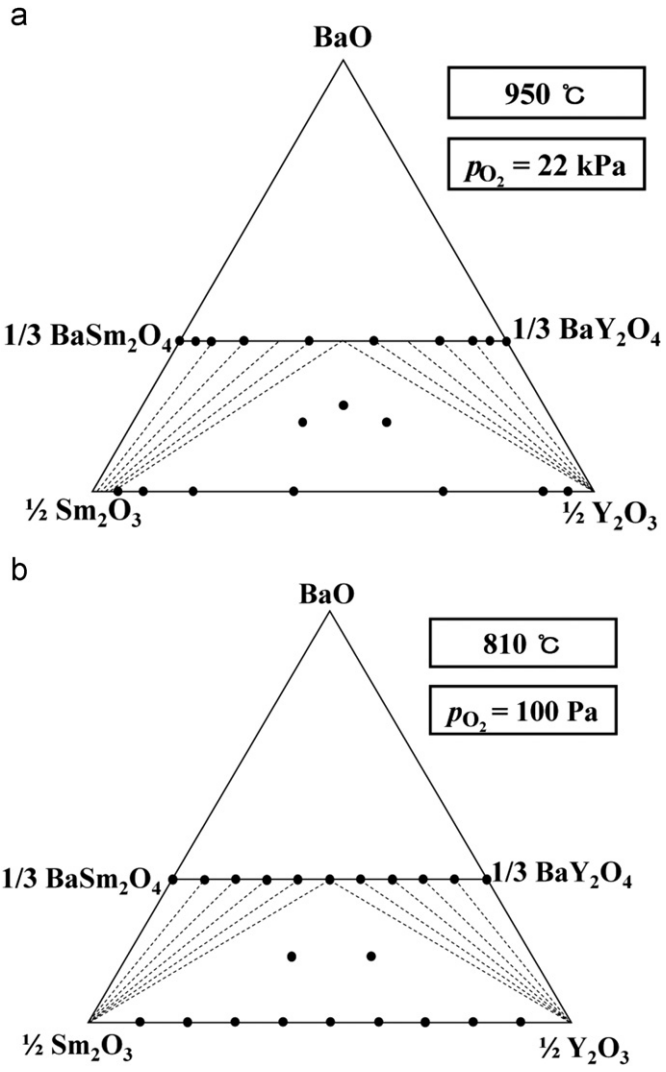

Fig. 3. Phase diagram of the $BaSm_2O_4$–BaY_2O_4–Sm_2O_3–Y_2O_3 system prepared in (a) pure air (p_{O_2} = 22 kPa, 950 °C) and (b) p_{O_2} = 100 Pa, 810 °C.

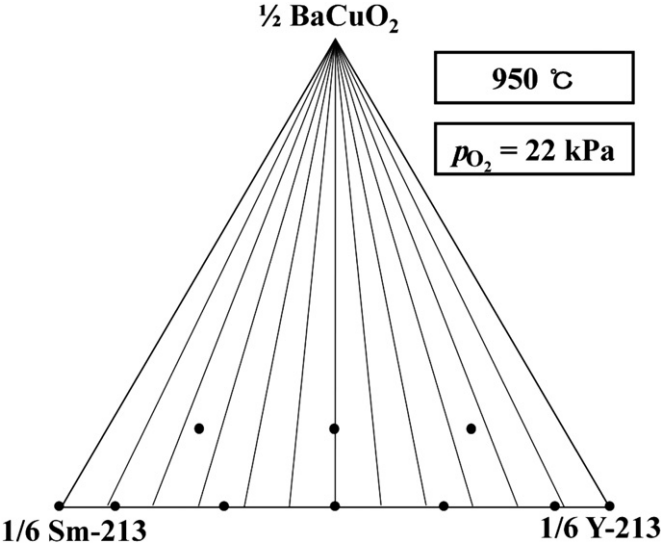

Fig. 4. Phase diagram of the $BaCuO_2$–$Ba_2SmCu_3O_{6+z}$–$Ba_2YCU_3O_{6+z}$ system prepared in pure air (p_{O_2} = 22 kPa, 950 °C). Phase diagram prepared in p_{O_2} = 100 Pa, 810 °C is similar.

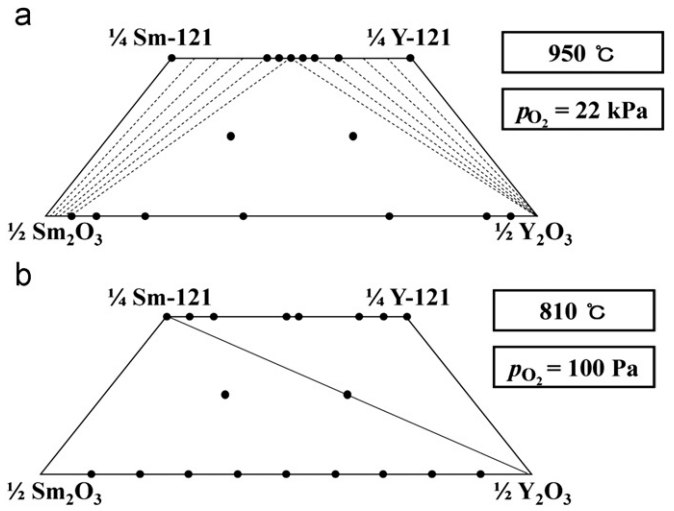

Fig. 5. Phase diagram of the $BaSm_2CuO_5$–BaY_2CuO_5–$Sm_2O_3-Y_2O_3$ system prepared in (a) pure air (p_{O_2} = 22 kPa, 950 °C) and (b) p_{O_2} = 100 Pa, 810 °C.

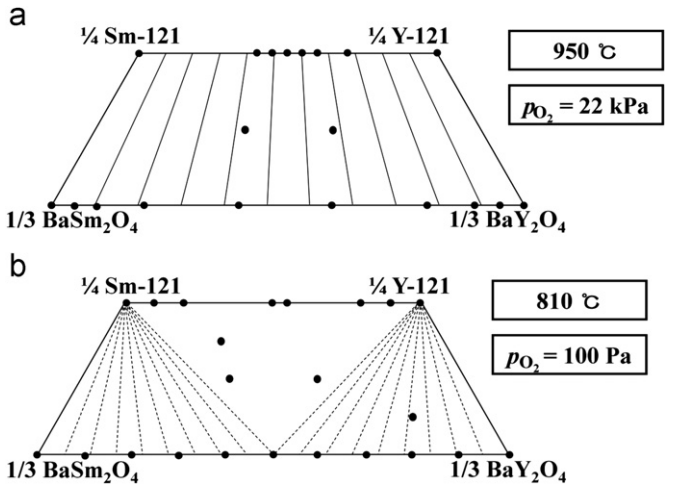

Fig. 6. Phase diagram of the $BaSm_2CuO_5$–BaY_2CuO_5–Sm_2O_3–Y_2O_3 system prepared in (a) pure air (p_{O_2} = 22 kPa, 950 °C) and (b) p_{O_2} = 100 Pa, 810 °C.

the Y_2O_3–CuO system while Sm_2CuO_4 is the stable phase found in the Sm_2O_3–CuO system.

Fig. 1a gives the phase diagram compatibilities of the Ba–Sm–Y–Cu–O system prepared at 810 °C under p_{O_2} = 100 Pa; the compatibilities at 950 °C in air are similar except for the absence of $BaCu_2O_2$. Fig. 1a shows an overview of Ba–Sm–Y–Cu–O phase relations in the BaO-poor region such that the compatibilities involving the Sm213–Y213–Y121–Sm121 plane are outlined. The detailed phase equilibria are more complicated in that the Sm213 and Y213 solid solutions extend below this plane. The general formula describing this solid solution is $(Ba_{2-x}Sm_x)(Sm_{1-y}Y_y)Cu_3O_{6+z}$, as shown schematically in Fig. 1b and c, and the solid solution limits are shown in more detail in Fig. 9. Thus, the $(Ba_{2-x}Sm_x)(Sm_{1-y}Y_y)Cu_3O_{6+z}$ solid solutions are connected to the Y121–Sm121 solid solutions by three-dimensional tie-line bundles, as indicated. The individual subsystems of the Ba–Sm–Y–Cu–O system, including the tie-line relationships and solid solution ranges of the different phases, are described separately in more detail in ternary oxide diagrams (Figs. 2–9).

3.1.1. *Ba–Sm–Y–Cu–O subsystems*

Figs. 2–8 give the phase equilibria of the subsystems of $Ba_{2-x}Sm_{1+x}Cu_3O_{6+z}$–$Ba_2YCu_3O_{6+z}$–$BaSm_2CuO_5$–$BaY_2CuO_5$, $BaSm_2O_4$–BaY_2O_4–$BaSm_2CuO_5$–BaY_2CuO_5, Sm_2CuO_4–$Y_2Cu_2O_5$–Sm_2O_3–Y_2O_3, $BaCuO_2$–$Ba_{2-x}Sm_{1+x}Cu_3O_{6+z}$–$Ba_2YCu_3O_{6+z}$, $BaSm_2CuO_5$–BaY_2CuO_5–Sm_2O_3–Y_2O_3, and $BaSm_2CuO_5$–BaY_2

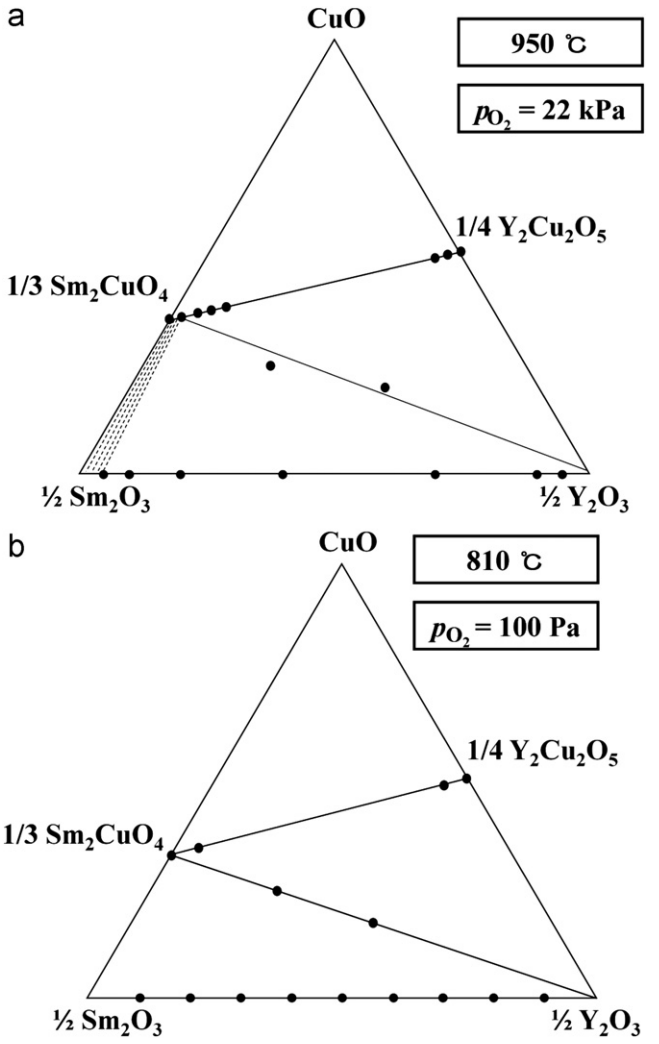

Fig. 7. Phase diagram of the Sm121–Y121–$BaSm_2O_4$–BaY_2O_4 system prepared in (a) pure air (p_{O_2} = 22 kPa, 950 °C) and (b) p_{O_2} = 100 Pa, 810 °C.

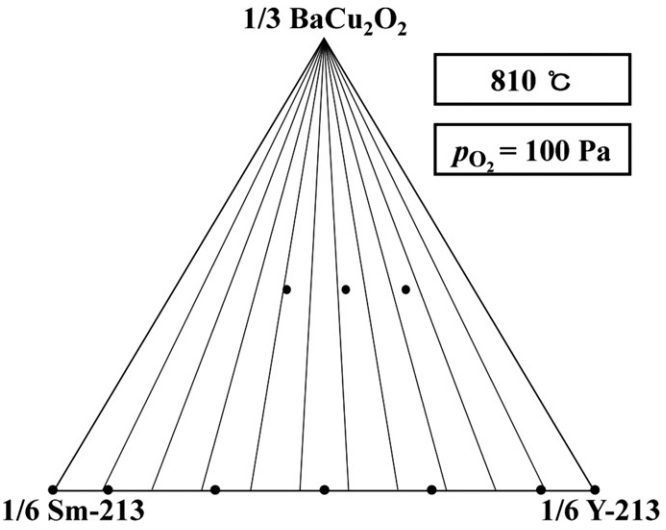

Fig. 8. Phase diagram of the $BaCu_2O_2$–$Ba_2SmCu_3O_{6+z}$–$Ba_2YCu_3O_{6+z}$ system in p_{O_2} = 100 Pa, 810 °C.

CuO_5–$BaSm_2O_4$–BaY_2O_4. Under $p_{O_2}=100$ Pa, an additional equilibrium assemblage of $BaCu_2O_2$–$Ba_{2-x}Sm_{1+x}Cu_3O_{6+z}$–$Ba_2YCu_3O_{6+z}$ was obtained as compared to the assemblages observed in air. While some of these systems have similar equilibrium relations, others are substantially different. For example, at 950 °C in pure air, the $Ba(Sm_xY_{2-x})CuO_5$ phase ('green phase') has a complete solid solution, however, at $p_{O_2}=100$ Pa and 810 °C, only a negligibly small extent was found. Because of this major difference, systems that involve the green phase solid solutions show substantially different equilibrium tie line distributions.

3.1.1.1. $Ba_2SmCu_3O_{6+z}$–$Ba_2YCu_3O_{6+z}$–$BaSm_2CuO_5$–BaY_2CuO_5. In pure air, both $(Ba_{2-x}Sm_x)(Sm_{1-y}Y_y)Cu_3O_{6+z}$ and $Ba(Sm_xY_{2-x})CuO_5$ phases form complete solid solutions. Tie-line bundles were found connecting these two series of solid solutions, as expected. However, under $p_{O_2}=100$ Pa and 810 °C, neither of the $BaSm_2CuO_5$ or BaY_2CuO_5 phases has a significant amount of solid solution, therefore different tie-lines relationships were found and as shown in Fig. 2a and b.

3.1.1.2. $BaSm_2O_4$–BaY_2O_4–Sm_2O_3–Y_2O_3. In pure air, Sm_2O_3 has a very small solid solution region with a limit at $(Sm_{0.8}Y_{0.2})_2O_3$ and Y_2O_3 is a point compound. The $Ba(Sm,Y)_2O_4$ phase forms a complete solid solution in pure air and in 100 Pa O_2. In pure air (Fig. 3a), the three-phase equilibrium is defined by $(Sm_{0.8}Y_{0.2})_2O_3$–$Ba(Sm_{0.5}Y_{0.5})_2O_4$–Y_2O_3. Under $p_{O_2}=100$ Pa (Fig. 3b), similar tie line bundles were found, except that no Sm_2O_3 solid solution was observed.

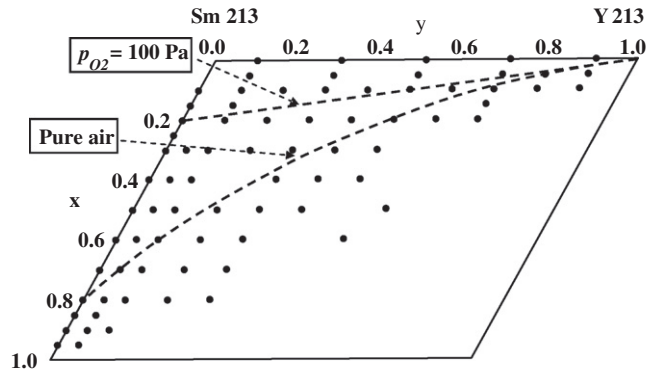

Fig. 9. The experimental boundaries of the solid solution regions of $(Ba_{2-x}Sm_x)(Sm_{1-y}Y_y)Cu_3O_{6+z}$ prepared in pure air ($p_{O_2}=22$ kPa, 950 °C) and in $p_{O_2}=100$ Pa, 810 °C.

3.1.1.3. $BaCuO_2$–$Ba_2SmCu_3O_{6+z}$–$Ba_2YCu_3O_{6+z}$. Under both conditions of pure air and $p_{O_2}=100$ Pa, tie-lines are found originating from $BaCuO_2$ and extending to the $(Ba_{2-x}Sm_x)(Sm_{1-y}Y_y)Cu_3O_{6+z}$ solid solutions, which are continuous (Fig. 4).

3.1.1.4. $BaSm_2CuO_5$–BaY_2CuO_5–Sm_2O_3–Y_2O_3. In pure air (Fig. 5a), $Ba(Sm_xY_{2-x})CuO_5$ forms a complete solid solution, but Sm_2O_3 only forms a small solid solution with Y_2O_3, with a limit at $(Sm_{0.8}Y_{0.2})_2O_3$. Under $p_{O_2}=100$ Pa (Fig. 5b), none of the $BaSm_2CuO_5$, BaY_2CuO_5, Sm_2O_3, or Y_2O_3 phases exhibits any significant amount of solid solution; a tie-line was found between $BaSm_2CuO_5$ and Y_2O_3 instead.

3.1.1.5. $BaSm_2CuO_5$–BaY_2CuO_5–$BaSm_2O_4$–BaY_2O_4. In pure air, both $Ba(Sm_xY_{2-x})CuO_5$ and $Ba(Sm,Y)_2O_4$ phases form complete solid solutions, therefore tie-line bundles run between the two solid solution series. However, under $p_{O_2}=100$ Pa, the extent of the solid solution range for $BaSm_2CuO_5$ and BaY_2CuO_5 is negligible. The approximate tie-line relationships between $Ba(Y,Sm)_2O_4$, $BaSm_2CuO_5$ and BaY_2CuO_5 are shown in Fig. 6a (pure air) and b ($p_{O_2}=100$ Pa).

3.1.1.6. Sm_2CuO_4–$Y_2Cu_2O_5$–Sm_2O_3–Y_2O_3. Results of the pure air experiments indicated that only Sm_2CuO_4 and Sm_2O_3 have solid solutions (with limits at $(Sm_{0.9}Y_{0.1})_2CuO_4$ and $(Sm_{0.8}Y_{0.2})_2O_3$), respectively. A tie-line was found between $(Sm_{0.9}Y_{0.1})_2CuO_4$ and Y_2O_3 (Fig. 7a). In the system prepared under $p_{O_2}=100$ Pa, the tie-line exists between Sm_2CuO_4 and Y_2O_3, with no solid solution detected (Fig. 7b).

3.1.1.7. $BaCu_2O_2$–$Ba_2SmCu_3O_{6+z}$–$Ba_2YCu_3O_{6+z}$. This equilibrium only exists in the reduced system of $p_{O_2}=100$ Pa, as $BaCu_2O_2$ is not stable in air. Since the $Ba_2SmCu_3O_{6+z}$ and $Ba_2YCu_3O_{6+z}$ phases form a complete solid solution, the tie-lines in this $BaCu_2O_2$–$Ba_2SmCu_3O_{6+z}$–$Ba_2YCu_3O_{6+z}$ system basically originate from

Table 1
Refined lattice parameters of the $Ba_{2-x}(Sm_{0.9+x}Y_{0.1})Cu_3O_{6+z}$ solid solution (in pure air, $p_{O_2}=0.22$ MPa, 950 °C).

x Space group	0.1 *Pmmm*(47)	0.2 *Pmmm*(47)	0.4 *P4/mmm*(123)	0.6 *P4/mmm*(123)
a (Å)	3.84752(5)	3.85958(8)	3.86932(4)	3.86505(5)
b (Å)	3.89755(10)	3.88677(12)		
c (Å)	11.7044(2)	11.6808(4)	11.6163(3)	11.5636(3)
V (Å^3)	175.52(2)	175.22(2)	173.92(1)	172.74(1)

Table 2
Refined lattice parameters of the orthorhombic 'green phase' (space group *Pnma* (no. 62)) in $Ba(Sm_xY_{2-x})CuO_5$ compounds (in pure air, $p_{O_2}=0.22$ MPa, 950 °C). The average lattice parameters of BaY_2CuO_5 ($x=0$) from 11 literature sources [26–36] are $a=12.174(14)$ Å, $b=5.657(3)$ Å, $c=7.131(3)$ Å, $V=491.28(71)$ Å^3.

x	0.2	0.4	0.8	1.0	1.6	1.8
a (Å)	12.1900(2)	12.2300(2)	12.2898(3)	12.31408	12.3889(4)	12.3994(3)
b (Å)	5.66263(10)	5.67703(9)	5.69958(13)	5.71002	5.7509(2)	5.75789(13)
c (Å)	7.13771(14)	7.15662(13)	7.1882(2)	7.20280	7.2616(3)	7.2714(2)
V (Å^3)	492.70(3)	496.89(2)	503.51(2)	506.45	517.38(1)	519.14(2)

$BaCu_2O_2$ and connect to the entire $(Ba_{2-x}Sm_x)(Sm_{1-y}Y_y)Cu_3O_{6+z}$ solid solution (Fig. 8).

3.2. Solid solution $(Ba_{2-x}Sm_x)(Sm_{1-y}Y_y)Cu_3O_{6+z}$

The experimental boundaries of the solid solution regions of $(Ba_{2-x}Sm_x)(Sm_{1-y}Y_y)Cu_3O_{6+z}$ prepared in pure air and in $p_{O_2}=100$ Pa are shown in Fig. 9. The single-phase boundaries are approximated by two curves. Along the vertical axis in the diagram (from top to bottom), an increase of x in $(Ba_{2-x}Sm_x)(Sm_{1-y}Y_y)Cu_3O_{6+z}$ indicates an increase of Sm substitution for the Ba site. The horizontal axis from left to right parallels an increasing amount of Y substitution on the Sm site. In other words, the end member at the upper right corner of the diagram is described as $Ba_2YCu_3O_{6+z}$, while at the upper left corner the end member is described as $Ba_2SmCu_3O_{6+z}$.

A comparison of the size of the solid solution indicates that it is larger under higher oxygen partial pressure. With $x=0$, $Ba_2(Sm_{1-y}Y_y)Cu_3O_{6+z}$ forms an entire solid solution across. With $x\neq 0$, complete solid solution formation between Sm and Y does not occur anymore. In general, it is observed that as Y substitutes into the larger Sm site, the lattice parameter decreases. Table 1 gives the lattice parameters of the series of $Ba_{2-x}(Sm_{0.9+x}Y_{0.1})$-$Cu_3O_{6+z}$ as a function of x. As the ionic size of Sm^{3+} is smaller than that of Ba^{2+} [22], the more the substitution of Sm into the Ba site, the smaller is the unit cell volume. A monotonic trend was observed. When $x=0.1$ and 0.2, the structure is orthorhombic ($Pmmm$) and with $x\geq 0.4$, the structure is tetragonal ($P4/mmm$). The structures of both the orthorhombic and tetragonal $Ba_2RCu_3O_{6+z}$ phases have been described in detail in the literature [23].

Standard X-ray powder patterns of selected members of $(Ba_{2-x}Sm_x)(Sm_{1-y}Y_y)Cu_3O_{6+z}$ were prepared and were submitted to ICDD for inclusion in the PDF (Table S4 and Table S5).

3.3. Solid solution $Ba(Sm_xY_{2-x})CuO_5$

The BaR_2CuO_5 (R=lanthanide) phase has two different structure types. When R is large (R=Nd and La), it forms the tetragonal brown phase structure [24–26]. For smaller size of lanthanide, (R=Sm–Lu), it forms the orthorhombic green phase structure.

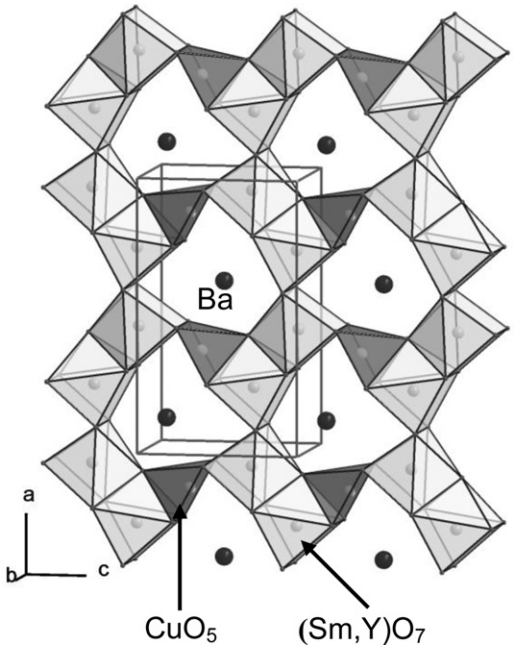

Fig. 10. Structure of $Ba(Sm_xY_{2-x})CuO_5$, showing the $[(Sm,Y)O_7]$ and $[CuO_5]$ polyhedra sharing edges to form a three-dimensional network whose cages are occupied by Ba ions.

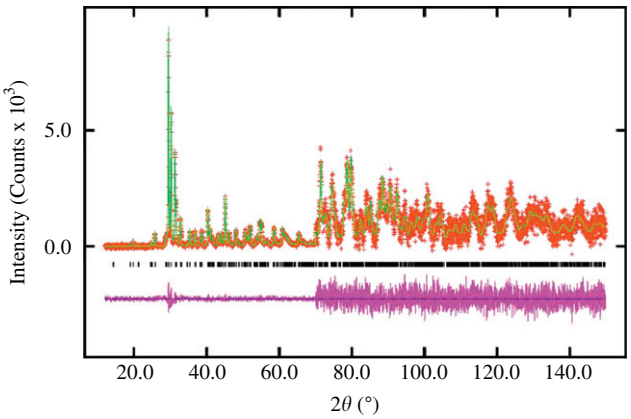

Fig. 11. Rietveld refinement for $Ba(Sm_{0.8}Y_{1.2})CuO_5$. The intermediate row of tick marks indicates the peak positions based on the experimental data of the top pattern. The difference pattern (lower pattern) is plotted at same scale as the top pattern up to 70° in 2θ. From $2\theta=70°$ on, the scale has been magnified 10 times. Refinement residues are $R_{wp}=0.0379$, $R_p=0.0288$, $R_F=0.0172$, $R_{F2}=0.0277$, and $\chi^2=1.637$.

$Ba(Sm_xY_{2-x})CuO_5$ is confirmed to be isostructural to the green phase BaR_2CuO_5 analogs [25,26]. When it was prepared in air, a complete solid solution was obtained. The cell parameters of representative members of this solid solution are given in Table 2, and indicate a linear trend. The average lattice parameters of the BaY_2CuO_5 end member obtained from 11 literature sources [26–36] are $a=12.174(14)$ Å, $b=5.657(3)$ Å, $c=7.131(3)$ Å, and $V=491.3(7)$ Å^3 (uncertainties are from cited sources). The solid solution extent was much smaller when $Ba(Sm_xY_{2-x})CuO_5$ was prepared in $p_{O_2}=100$ Pa.

The general structure of $Ba(Sm_xY_{2-x})CuO_5$ consists of a three-dimensional network of interconnected $[(Sm,Y)O_7]$, $[BaO_{11}]$, and $[CuO_5]$ polyhedra, and is analogous to the Y analog [37] (Fig. 10). Standard reference patterns for selected members of $Ba(Sm_xY_{2-x})CuO_5$ ($x=0.2$, 0.4, 0.8, 1.6, and 1.8) have been prepared and submitted to ICDD. Fig. 11 gives an example of the Rietveld patterns used to prepare the standard X-ray data.

4. Summary

Since an understanding of the detailed multi-component phase equilibrium relationships in the vicinity of the superconductor solid solution, $(Ba_{2-x}Sm_x)(Sm_{1-y}Y_y)Cu_3O_{6+z}$, will allow improvement of coated conductor processing, we have determined the phase compatibilities of $(Ba_{2-x}Sm_x)(Sm_{1-y}Y_y)Cu_3O_{6+z}$ in the quaternary Ba–Sm–Y–Cu–O oxide system under $p_{O_2}=100$ Pa (810 °C) and in pure air ($p_{O_2}=22$ kPa, 950 °C). The corresponding complex phase relationships of the Ba–Sm–Y–Cu–O system near the BaO-poor region have also been determined. As mixed lanthanide systems are increasingly important for coated conductor applications, it is imperative that the phase equilibria information of other mixed lanthanide systems such as that of the (Eu,Y), (Nd,Y), and (Gd,Y)-systems be available in the near future.

Acknowledgments

The authors acknowledge the partial financial support from the US Department of Energy and also from the International Centre for Diffraction Data. Mr. N. Swanson is thanked for his graphical assistance.

Appendix A. Supplemental Information

Supplementary data associated with this article can be found in the online version at doi:10.1016/j.jssc.2010.09.001.

References

[1] A.P. Malozemoff, D.T. Verebelyi, S. Fleshler, D. Aized, D. Yu, Physica C 386 (2003) 424–430.
[2] M.W. Rupich, W. Zhang, X. Li, T. Kodenkandath, D.T. Verebelyi, U. Schoop, C. Thieme, M. Teplitsky, J. Lynch, N. Nguyen, E. Siegal, J. Scudiere, V. Maroni, K. Venkataraman, D. Miller, T.G. Holesinger, Physica C 412–414 (2004) 877–884.
[3] A. Goyal, D.P. Norton, J.D. Budai, M. Paranthaman, E.D. Specht, D.M. Kroeger, D.K. Christen, Q. He, B. Saffian, F.A. List, D.F. Lee, P.M. Martin, C.E. Klabunde, E. Hartfield, V.K. Sikka, Appl. Phys. Lett. 69 (1996) 1795–1797.
[4] A. Goyal, P. Paranthaman, U. Schoop, MRS Bull. 29 (2004) 552–561.
[5] P.N. Arendt, S.R. Foltyn, L. Civale, R.F. DePaula, P.C. Dowden, J.R. Groves, T.G. Holesinger, Q.X. Jia, S. Kreiskott, L. Stan, I. Usov, H. Wang, J.Y. Coulter, Physica C 412–414 (2004) 795–800.
[6] S.R. Foltyn, E.J. Peterson, J.Y. Coulter, P.N. Arendt, Q.X. Jia, P.C. Dowden, M.P. Maley, X.D. Wu, D.E. Peterson, J. Mater. Res. 12 (1997) 2941–2946.
[7] Y. Yamada, A. Ibi, H. Fukushima, R. Kuriki, S. Miyata, K. Takahashi, H. Kobayashi, S. Ishida, M. Konishi, T. Kato, T. Hirayama, Y. Shiohara, Physica C 445–448 (2006) 504–508.
[8] R. Feenstra, T.B. Lindemer, J.D. Budai, M.D. Galloway, J. Appl. Phys. 69 (1991) 6569.
[9] V. Selvamanickam, H.G. Lee, Y. Li, X. Xiong, Y. Qiao, J. Reeves, Y. Xie, A. Knoll, K.R. Lenseth, Physica C 392–396 (2003) 859–862.
[10] V. Selvamanickam, Y. Chen, X. Xiong, Y.Y. Xie, J.L. Reeves, X. Zhang, Y. Qiao, K.R. Lenseth, R.M. Schmidt, A. Rar, D.W. Hazelton, K. Tekletsadik, IEEE Trans. Appl. Superconductivity 17 (2) (2007) 3231–3234.
[11] P.M. Mankiewich, J.H. Scofield, W.J. Skocpol, R.E. Howard, A.H. Dayem, E. Good, Appl. Phys. Lett. 51 (21) (1987) 1753–1755.
[12] S.-W. Chan, B.G. Bagley, L.H. Greene, M. Giroud, W.L. Feldmann, K.R. Jenkin II, B.J. Wilkins, Appl. Phys. Lett. 53 (15) (1988) 1443–1445.
[13] P.C. McIntyre, M.J. Cima, J. Mater. Res. 9 (9) (1994) 2219–2230.
[14] P.C. McIntyre, M.J. Cima, A. Roshko, J. Appl. Phys. 77 (10) (1995) 5263–5272.
[15] J.L. MacManus-Driscoll, B. Maiorov, J. Durrell, S. Foltyn, Q.X. Jia, L. Civale, H. Wang, A. Kursumovic, D.E. Peterson, Superconductivity Sci. Technol. 19 (2006) S55–S59.
[16] PDF, Powder Diffraction File, produced by ICDD, Newtown Square, 12 Campus Blvd., Newtown Square, PA 19073-3273.
[17] J.J. Ritter, Powder Diffraction 3 (1) (1988) 30.
[18] H.M. Rietveld, J. Appl. Crystallogr. 2 (1969) 65–71.
[19] A.C. Larson, R.B. von Dreele, GSAS-General Structure Analysis System, US Government Contract (W-7405-ENG-36) by the Los Alamos National laboratory, which is operated by the University of California for the US Department of Energy, 1992.
[20] W. Wong-Ng, L.P. Cook, J. Suh, J.A. Kaduk, Physica C 405 (2004) 47–58.
[21] W. Wong-Ng, L.P. Cook, J. Suh, Physica C 377 (2002) 107–113.
[22] R.D. Shannon, Acta Crystallogr. A32 (1976) 751–767.
[23] Y. Le Page, T. Siegrist, S.A. Sunshine, L.F. Schneemeyer, D.W. Murphy, S.M. Zahurak, J.V. Waszczak, W.R. McKinnon, J.M. Tarascon, G.W. Hull, L.H. Green, Phys. Rev. B36 (1987) 3617–3621.
[24] J.K. Stalick, W. Wong-Ng, Mater. Lett. 9 (10) (1990) 401.
[25] W. Wong-Ng, B. Paretzkin, E.R. Fuller Jr., J. Solid State Chem. 85 (1990) 117–132.
[26] W. Wong-Ng, M.A. Kuchinski, H.F. McMurdie, B. Paretzkin, Powder Diffraction 4 (1) (1989) 2–8.
[27] C. Michel, B. Raveau, J. Solid State Chem. 43 (1982) 73–80.
[28] N.L. Ross, R.J. Angel, L.W. Finger, R.M. Hazen, C.T. Prewitt, ACS Symp. Ser. 351 (1987) 164–172.
[29] H. Fjellvag, P. Karen, A. Kjekshus, Acta Chem. Scand. 41 (1987) 283–293.
[30] R.M. Hazen, L.W. Finger, R.J. Angel, C.T. Prewitt, N.L. Ross, H.K. Mao, C.G. Hadidiacos, P.H. Hor, R.L. Meng, C.W. Chu, Phys. Rev. B35 (1987) 7238–7241.
[31] S.F. Watkins, F.R. Fronczek, K.S. Wheelock, R.G. Goodrich, W.O. Hamilton, W.W. Johnson, Acta Crystallogr. Sect. C: Cryst. Struct. Commun. 44 (1988) 3–6.
[32] S. Sato, I. Nakada, Acta Crystallogr. Sect. C: Cryst. Struct. Commun. 45 (1989) 523–525.
[33] B.A. Hunter, S.L. Town, R.L. Davis, G.J. Russell, K.N.R. Taylor, Physica C 161 (1989) 594–597.
[34] A. Salinas-Sanchez, J.L. Garcia-Munoz, J. Rodriguez-Carvajal, R. Saez-Puche, J.L. Martinez, J. Solid State Chem. 100 (1992) 201–211.
[35] R.H. Buttner, E.N. Maslen, Acta Crystallogr. 49 (1993) 62–66.
[36] R. Hsu, E.N. Maslen, N. Ishizawa, Acta Crystallogr. B52 (1996) 569–575.
[37] G. Liu, Q. Huang, J. Kaduk, Z. Yang, C. Lucas, W. Wong-Ng, J. Solid State Chem. 181 (2008) 3236–3242.